Orbital ordering in $LaMnO_3$ Investigated by Resonance Raman Spectroscopy

R. Krüger,[1] B. Schulz,[1] S. Naler,[1] R. Rauer,[1] D. Budelmann,[1] J. Bäckström,[1] K. H. Kim,[2] S-W. Cheong,[3] V. Perebeinos,[4] and M. Rübhausen[1]

[1]*Institut für Angewandte Physik, Universität Hamburg, Jungiusstraße 9, D-20355 Hamburg, Germany*
[2]*National High Magnetic Field Laboratory, MS-E536 LANL, Los Alamos, New Mexico 87545, USA*
[3]*Department of Physics and Astronomy, Rutgers University, Piscataway, New Jersey 08854, USA*
[4]*Brookhaven National Laboratory, Upton, New York 11973, USA*

(Received 15 June 2003; published 3 March 2004)

Orbital ordering leads to an unconventional excitation spectrum that we investigate by resonance Raman scattering using incident photon energies between 1.7 and 5.0 eV. We use spectral ellipsometry to determine the corresponding dielectric function. Our results show resonant behavior of the phonon Raman cross section when the laser frequency is close to the orbiton-excitation energy of 2 eV in $LaMnO_3$. We show an excellent agreement between theoretical calculations based on the Franck-Condon mechanism activating multiphonon Raman scattering in first order of the electron-phonon coupling and the experimental data of phonons with different symmetries.

DOI: 10.1103/PhysRevLett.92.097203 PACS numbers: 75.47.Lx, 63.20.Ls, 71.27.+a, 78.30.–j

Signatures of orbital ordering have been unambiguously identified by elastic x-ray techniques [1]. However, much debate has been recently ignited about the dominant energy scale driving the formation of an orbital-ordered state and its corresponding excitation spectrum [2–4]. Two fundamentally different concepts lead to energy scales that differ by 1 order of magnitude. In one scenario the electron-phonon coupling drives the orbital ordering leading to a typical energy scale of the orbiton mode given by the strength of the electron-phonon (e-ph) coupling, $\sim$1.5 eV [3,5,6], whereas the second scenario predicts smaller energies $\sim$0.16 eV due to renormalization related to the strength of the Coulomb on-site repulsion [5–7]. Inelastic resonant scattering of visible and soft x-ray photons are currently strongly involved in tracking down the orbiton mode yielding also two fundamentally different assignments that differ by 1 order of magnitude in energy.

Here we present a resonant inelastic light-scattering study with excitation energies ranging from near IR (1.7 eV) to deep UV (5 eV) in order to investigate the matrix elements related to two important energies at around 2 and 4.4 eV, representing the Jahn-Teller (JT) and charge-transfer (CT) gaps, respectively [8,9]. Our experimental results are complemented by a symmetry-dependent calculation of the one- and two-phonon scattering cross sections within the Franck-Condon (FC) mechanism allowing for enhanced multiphonon scattering in the orbitally ordered state. Our main findings are (i) the one- and two-phonon excitation spectrum shows sharp resonances for incident photon energies close to the JT gap at 2 eV and at the CT gap at 4.4 eV; (ii) the one-phonon spectrum shows resonance profiles that strongly depend on the symmetry of the phonon modes. The vibrational oxygen breathing mode at 655 cm^{-1} (81 meV) resonates strongly at the CT gap. Phonon modes at 611 cm^{-1} (76 meV) and at 496 cm^{-1} (62 meV) show their strongest resonance at the JT gap; (iii) these three phonon modes with their individual resonance properties yield a complicated two-phonon spectrum between 1100 and 1300 cm^{-1}; (iv) we find good agreement between the symmetry-dependent resonance properties of the three main oxygen phonon modes and theoretical calculations based on the FC mechanism in the orbitally ordered state. This is indicative of an orbital-ordered state that is formed to a large extent by the e-ph interaction. The FC mechanism predicts the correct resonance energies of the JT modes at 2 eV and the correct one- to two-phonon ratios.

Previous Raman scattering studies have been performed with visible incident photon energies showing an excellent agreement with the assignment of Iliev *et al.* in the one-phonon spectrum between 80 and 640 cm^{-1} [10]. More controversial is the assignment of modes in the two-phonon spectral range between 1100 and 1300 cm^{-1} with a claim that a mode at 160 meV is not related to a two-phonon peak but to an orbital wave or orbiton [7]. This claim has been challenged by Grüninger *et al.*, who identify the 1300 cm^{-1} mode as an overtone of the highest energy one-phonon peak in the IR spectrum. However, due to possible symmetry breaking, the parity argument discriminating Raman and IR data might not hold and the situation remains unclear [11]. Our resonance study reveals the inelastic light-scattering matrix elements and shows that the resonances of the one-phonon modes are also visible in the two-phonon spectra, strongly suggesting a phononic origin of the peaks between 1100 and 1300 cm^{-1}.

The inelastic light-scattering experiments have been performed on a novel Raman spectrometer (McPherson) equipped with a UV-sensitive charge-coupled device and with a reflecting objective in a Cassegrain design. The

primary mirror is an on-axis parabola with a numerical aperture of 0.5 [12]. The incident light is generated by Ar^+ and Kr^+ lasers with an intracavity frequency doubler for wavelengths below 275 nm. The incident light passes optical elements (premonochromator, scrambler, spatial filter, and polarizer) and is focused by the the reflecting objective that also couples the scattered light into the spectrometer. Because of the diffraction limited imaging we determine the size of the spot by the size of the pinhole in the spatial filter. We have used a 30 μm spot and 8 mW of power on the sample in order to avoid any significant heating. The Raman spectrometer has been calibrated by two double Ulbricht sphere systems for visible and ultraviolet wavelengths (gigahertz). Measurements have been performed on single crystals at room temperature in a temperature ($22\pm0.3\,^{\circ}$C) and humidity ($45\%\pm3\%$) controlled clean room (class 100) and in backscattering configuration with parallel polarization for the incident and scattered light along the in-plane crystal axis probing phonons of A_g and B_{2g} symmetry. The spectra are corrected for integration time, incident power, the wavelength dependent penetration depth, and reflection coefficient as determined by the dielectric function measured by spectroscopic ellipsometry (Sentech Instruments). The largest error of the experiment is given by the chromatic aberrations in the spatial filter with a change of the incident photon energy. By repeated measurements of Si-reference spectra across our full spectral range we estimate a maximum error in the UV of less than 10%. Other error sources such as the uncertainty of the dielectric function or the stability of the laser yield errors of the order of less than 1%.

In Fig. 1 we present Raman spectra for incident photon energies from 1.96 to 4.5 eV, in the one- (a) and two-phonon (b) spectral ranges. For previously used incident photon energies (1.96 and 2.34 eV) we see the well-known phonon modes of A_g and B_{2g} symmetry. Between 200 and 400 cm^{-1} the spectra show strong signals from the in-phase y rotation $A_g(2)$ at 257 cm^{-1}, and the out-of-phase x rotation $A_g(4)$ at 284 cm^{-1}. Both modes show a weak signal with visible excitation energies and strong resonance enhancements for deep-UV excitation, clearly supporting their assignment as rotational vibrations that are not coupling strongly to the JT e_g levels. There is the appearance of an additional mode in the deep UV around 448 cm^{-1} (4.1 and 4.5 eV) that has not been observed before, showing an analogous resonance behavior to the rotational modes. The higher-energy oxygen modes are observed between 496 and 655 cm^{-1}. Especially, the in-phase stretching $B_{2g}(1)$ mode at 611 cm^{-1} shows a single pronounced resonance at around 2 eV as it strongly modulates the JT levels. Phonons around 496 and 655 cm^{-1} resonate towards 2 and 4.4 eV. This strongly suggests that the 496 cm^{-1} phonon is not a pure rotational or bending mode of the oxygen cage but rather related to the $A_g(1)$ in-phase stretching mode and

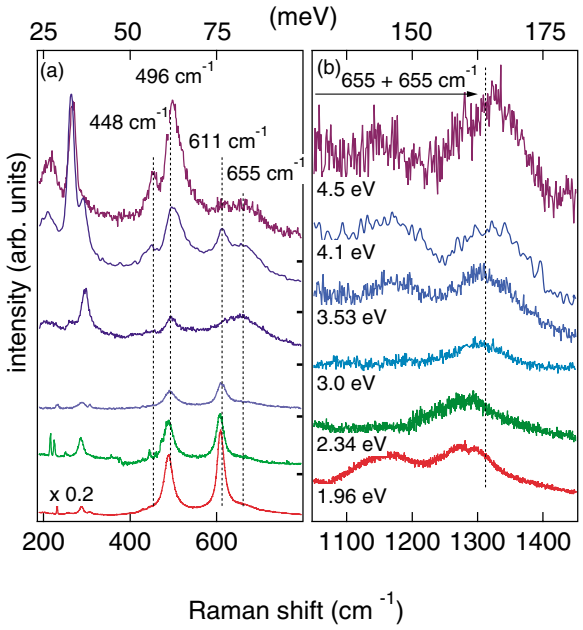

FIG. 1 (color online). Experimental spectra showing the oxygen vibrations of the distorted MnO_6 octahedra in the one- (a) and two-phonon (b) regions.

that the new mode at 448 cm^{-1} is most probably the bending $A_g(3)$ vibration [10].

Figure 1(b) displays the two-phonon region for the same incident photon energies as Fig. 1(a). Overall we find two-phonon features that correspond to the energy range between 1100 and 1300 cm^{-1}, i.e., about twice 611 and 655 cm^{-1}. The more complicated two-phonon spectrum typical for the visible spectral range simplifies when the 611 cm^{-1} mode disappears in the deep UV, leaving alone a single peak at 1300 cm^{-1}. This two-phonon peak exhibits the same matrix elements as the 655 cm^{-1} phonon resonating towards the charge-transfer gap at 4.4 eV.

The details of the observed resonances for the three JT related phonons, as well as the resonances of the two-phonon peak around 1300 cm^{-1}, are shown in Figs. 2(a) and 2(b), respectively. The most important observations in Fig. 2(a) are that all three one-phonon modes resonate at the same energy of 2.05 eV with a FWHM of 0.65 eV, as derived from a fit of a Gaussian profile (solid line) to the data points. The second resonance around the charge-transfer energy is visible in the 655 cm^{-1} and in the 496 cm^{-1} phonon with slightly shifted energies (4.1 to 4.4 eV), but with the same width of the resonances of 1.32 eV. The dielectric function shows that the first resonance corresponds to the JT gap and that absorption levels at 2.2 and 2.5 eV are not involved in the resonance process. Moreover, we find the strong resonance of the CT level buried in a monotonically increasing absorption band. The shift in resonance energy of the 496 and 655 cm^{-1} phonons could be due to a symmetry-dependent renormalization of the matrix elements or due to the presence of additional CT processes such as a combination of O p

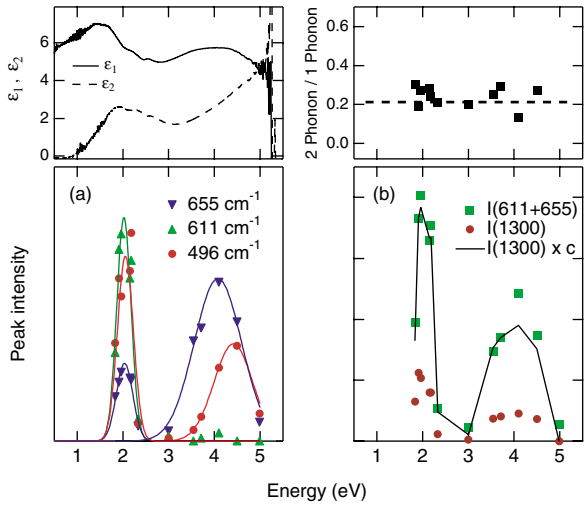

FIG. 2 (color online). Resonance profiles of the one-phonon excitations (a) and the comparison between the resonance profiles of the one- and two-phonon excitations (b). The inset in (a) shows ϵ_1 (solid line) and ϵ_2 (dashed line) of the dielectric function and in (b) the ratio of the one- to two-phonon intensities.

to Mn d (crystal-field splitting) and Mn d to nearest neighbor Mn d transitions (correlations).

Figure 2(b) shows the integrated intensity of the two one-phonon peaks at 611 and 655 cm^{-1} as well as that of the two-phonon peak. The solid line is the two-phonon peak intensity multiplied by a factor of 4.166. The inset shows the constant ratio of the one- to two-phonon peak intensities between 1.8 and 5 eV. This indicates that the feature at 1300 cm^{-1} is indeed a two-phonon peak as such a behavior of one- to two-phonon resonances is also typical for, e.g., Si [13].

In the conventional Raman scattering process of phonons, where electronically excited states do not alter atomic positions, the intensity of the n-phonon peak is proportional to g^{2n}, where g is the e-ph interaction and is a small number of $\approx 10^{-1}$–10^{-2}. When the oscillator potential curves of ground and excited states are displaced, vibrational Raman scattering is activated by a FC mechanism. In the first step of the FC Raman process, the incident photon creates an orbital defect in the ordered JT ground state. This Frenkel exciton, or orbiton, is self-trapped by an oxygen rearrangement from the JT state [6]. The FC principle has the oxygen positions undistorted during optical excitation, producing a vibrationally excited state of the orbiton. In the second step of the Raman process, this virtual excitation decays back to the orbital, but not necessarily to the vibrational, ground state. The amplitude for ending in a vibrationally excited state is determined by displaced-oscillator overlap integrals allowing n-phonon resonant Raman scattering with intensities proportional to g^n [14].

Perebeinos and Allen gave a derivation of the resonant multiphonon Raman cross section [15] with a net result:

$$\begin{aligned}\frac{\partial^2 \mathrm{R}^n_{\alpha\beta}}{\partial\omega_R \partial\Omega} &= S\left|\sum_{m=0}^{\infty}\frac{\hbar\omega A^n_{\alpha\beta}(m)}{\Delta + m\hbar\omega - \hbar\omega_L + i\gamma_m}\right|^2 \\ &\quad\times \delta(\omega_R - n\omega), \\ A^n_{\alpha\beta}(m) &= \sum_{\{m'\}}\delta(m - N\{m'\})\langle n|u_\alpha + u_{-\alpha}|m'\rangle \\ &\quad\times \langle m'|u_\beta + u_{-\beta}|0\rangle,\end{aligned} \tag{1}$$

where $S = (\sigma_0\omega_S)^2/\omega_L^2$ and $\sigma_0 = r_e^2 = e^2/m_e c^2$ is the Compton cross section. The summation goes over all electronic states and corresponding vibrational quanta $\{m\}$. $N\{m\} = m_x + m_y + m_z + m_{-x} + m_{-y} + m_{-z}$ is the total number of vibrational quanta of the six neighboring oxygens. To model the damping term γ_m of the vibrational level m, we use the expression $\gamma_m = \gamma_0\sqrt{m+1}$, as in a sequence of convolved Gaussians, intended to mimic the local densities of phonon states on oxygen atoms. The induced dipole matrix elements and displacements are measured in units of $(m_e M\omega^2)^{1/2}$ and $\sqrt{\hbar/M\omega}$, respectively. The ground state couples to excited electronic states by the electron-radiation Hamiltonian $(\hat{p}\cdot\vec{A})$ responsible for resonant Raman scattering. It has been suggested [6,15] that this transition becomes allowed because of asymmetric oxygen fluctuations [16].

In the previous work [15], the symmetry of the excited phonon in the final state was not taken into account. Here we allow the final state $|0, n\rangle$ to have an electronic ground state plus n vibrational A_g (Q_2) phonons:

$$|0, n\rangle = \frac{[\frac{1}{2}(a_x^\dagger - a_{-x}^\dagger - a_y^\dagger + a_{-y}^\dagger)]^n}{\sqrt{n!}}|0, 0\rangle. \tag{2}$$

To evaluate vibrational integrals $A^n_{\alpha,\beta}(m)$ one needs the expressions for overlap integrals of displaced harmonic oscillators [14,15]. There are only diagonal contributions to the one- and two-phonon Raman cross sections:

$$\begin{aligned}A^1_{\alpha\beta}(m) &= \delta_{\alpha,\beta}\frac{e^{-\Delta}\Delta^m}{m!}\frac{m}{\Delta^{3/2}}(\Delta - m + 1), \\ A^2_{\alpha\beta}(m) &= \delta_{\alpha,\beta}\frac{e^{-\Delta}\Delta^m}{m!}\frac{m}{\sqrt{2}\Delta^2} \\ &\quad\times[\Delta^2 - 2\Delta(m-1) + (m-1)(m-2)].\end{aligned} \tag{3}$$

The resonance of the matrix element is shown in Fig. 3 for $\gamma_0 = 120$ cm^{-1}. A pronounced resonant behavior is predicted when the laser frequency ω_L approaches the orbiton energy 2Δ. The resonance position is fixed by the dielectric function (Fig. 2) at 2 eV. Within the FC mechanism the width of the resonance is given by Δ and is 1 eV. The experimental results of the resonance profiles of the one- and two-phonon peaks show a remarkable agreement between experiment and theory given the fact that none of the theoretical parameters is fixed by a fit to the experimental phonon resonances. The ratio between the one- and two-phonon scattering cross sections as well as their

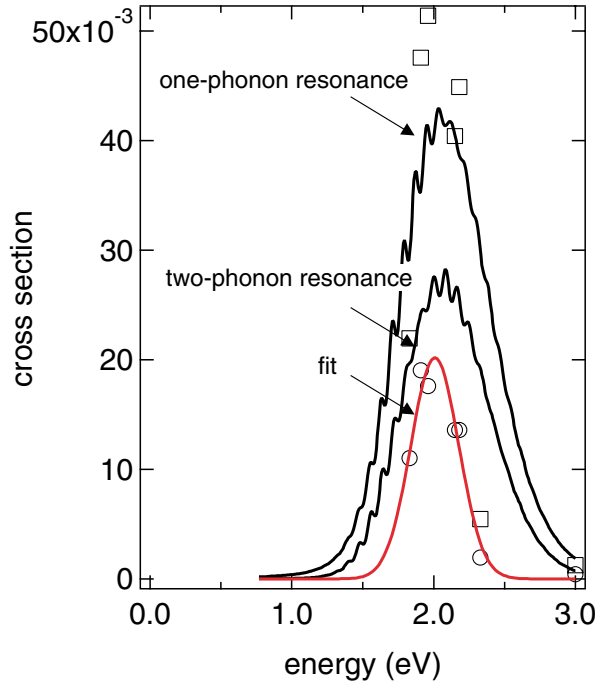

FIG. 3 (color online). Solid lines show the resonance profiles at orbiton energy of the one- and two-phonon peaks according to the Franck-Condon mechanism. Markers represent experimental data for the 611 cm^{-1} one-phonon (squares) and the 1300 cm^{-1} two-phonon (circles) resonance.

peak positions agree with the theoretical expectations. The most obvious difference is the much sharper experimental resonance data and could be resolved by considering a second gap contribution maybe due to the additional crystal-field splitting of the e_g orbitals by strain and electronic correlations neglected in our calculations [17].

The absolute value of the Raman cross section (in units of σ_0) according to Eq. (1) is a product of the resonant function S^n and the dipole matrix elements measured in units of $(m_e M\omega^2)^{1/2}$. The model Hamiltonian [2,5] predicts a minimum at amplitude $Q = \sqrt{A_g^2 + B_{2g}^2}$ of the cooperative oxygen distortions. The minimum $(B_{2g}, A_g) = Q(\cos\Theta, \sin\Theta)$, however, is degenerate with respect to angle Θ.

The results for the vibrational overlap integrals $A^n_{\alpha,\beta}$ Eq. (3) and resonances in Fig. 3 are reported for a purely B_{2g}-type distorted ground state ($\Theta = 90°$). The absolute value of the dipole matrix elements can be taken from the optical conductivity oscillator strength or density functional theory (DFT) calculations. The measured spectral weight of the lowest broad line centered at 2 eV corresponds to $f_{\rm exp} = 0.113$ [8], $f_{\rm exp} = 0.16$ [9], and $f_{\rm exp} = 0.22$ [18], which agrees with the DFT result $f_{\rm DFT} = 0.26$ [15]. The calculations of the resonant Raman scattering of the A_g-type phonons gives zero intensity for the first and second order Raman processes in the B_{2g}-type distorted ground state ($\Theta = 90^{\circ}$). From the fact that the resonances of the 611 and 496 cm^{-1} modes are comparable in strength (see Fig. 2) we can confirm that the angle Θ is much different from 90° in agreement with the prediction for the anisotropy of the optical conductivity $\sigma_{xx}/\sigma_{zz} = 0.5[2 + \cos(2\Theta)]/[1 - \cos(2\Theta)]$ and results from Tobe *et al.* [18] suggesting $\Theta \approx 36°$.

In summary, we have shown the efficiency of inelastic light scattering to study the interplay between electronic structure and orbital ordering in $LaMnO_3$. We find that the orbital ordering is to a large extent driven by the electron-phonon interaction with some additional electronic contribution. We find a remarkably good agreement between the experimental results and a theory based on the Franck-Condon mechanism.

We acknowledge many stimulating discussions with M. V. Klein, S. L. Cooper, U. Merkt, M. V. Abrashev, and P. Allen. We thank McPherson (Erik Schoeffel and Art Mayhill) for the excellent collaboration. We are supported by DFG Ru773/2-2, by Ru773/2-3, by GrK "Physik nanostrukturierter Festkörper," by NSF-DMR-0080008 (S-W. C.), and by U.S. DOE DE-AC02-98CH10886 (V. P.). K. H. K. is partially supported by CSCMR through the KOSEF.

[1] Y. Murakami *et al.*, Phys. Rev. Lett. **81**, 582 (1998).
[2] A. J. Millis, Phys. Rev. B **53**, 8434 (1996).
[3] A. J. Millis, B. I. Shraiman, and R. Mueller, Phys. Rev. Lett. **77**, 175 (1996).
[4] E. Dagotto, T. Hotta, and A. Moreo, Phys. Rep. **344**, 1 (2001).
[5] P. B. Allen and V. Perebeinos, Phys. Rev. B **60**, 10 747 (1999).
[6] P. B. Allen and V. Perebeinos, Phys. Rev. Lett. **83**, 4828 (1999).
[7] E. Saitoh *et al.*, Nature (London) **410**, 180 (2001).
[8] J. H. Jung *et al.*, Phys. Rev. B **57**, 11 043 (1998).
[9] J. H. Jung *et al.*, Phys. Rev. B **55**, 15 489 (1997).
[10] M. N. Iliev *et al.*, Phys. Rev. B **57**, 2872 (1998).
[11] M. Grüninger *et al.*, Nature (London) **418**, 39 (2002).
[12] On the entrance objective, see, e.g., Photonics Spectra 159 (October 2002).
[13] J. R. Renucci, R. N. Tyte, and M. Cardona, Phys. Rev. B **11**, 3885 (1975).
[14] L. L. Kruschinskii and P. P. Shorygin, Opt. Spectrosc. (USSR) **11**, 12 (1961); **11**, 80 (1961).
[15] V. Perebeinos and P. B. Allen, Phys. Rev. B **64**, 085118 (2001).
[16] Alternatively, *d-d* transitions could be also activated by static disorder of the oxygen octahedra or a quasielastic contribution.
[17] J. van den Brink, Peter Horsch, and Andrzej M. Oles, Phys. Rev. Lett. **85**, 5174 (2000).
[18] K. Tobe *et al.*, Phys. Rev. B **64**, 184421 (2001).